
Article

Not peer-reviewed version

Understanding the Origin of Luminescence in Porous Organosilica Films with Various Organic Components

[Md Rasadujjaman](#)^{*} , Jinming Zhang , Dmitry A. Spassky , Sergej Naumov , [Alexey S. Vishnevskiy](#) , [Konstantin A. Vorotilov](#) , Jiang Yan , [Jing Zhang](#) , [Mikhail R. Baklanov](#)

Posted Date: 20 March 2023

doi: 10.20944/preprints202303.0348.v1

Keywords: low-k dielectrics; organosilica glass; interconnects; photoluminescence; oxygen deficient centers



Preprints.org is a free multidiscipline platform providing preprint service that is dedicated to making early versions of research outputs permanently available and citable. Preprints posted at Preprints.org appear in Web of Science, Crossref, Google Scholar, Scilit, Europe PMC.

Copyright: This is an open access article distributed under the Creative Commons Attribution License which permits unrestricted use, distribution, and reproduction in any medium, provided the original work is properly cited.

Disclaimer/Publisher's Note: The statements, opinions, and data contained in all publications are solely those of the individual author(s) and contributor(s) and not of MDPI and/or the editor(s). MDPI and/or the editor(s) disclaim responsibility for any injury to people or property resulting from any ideas, methods, instructions, or products referred to in the content.

Article

Understanding the Origin of Luminescence in Porous Organosilica Films with Various Organic Components

Md Rasadujjaman ^{1,2,*}, Jinming Zhang ¹, Dmitry A. Spassky ^{3,4}, Sergej Naumov ⁵, Alexey S. Vishnevskiy ⁶, Konstantin A. Vorotilov ⁶, Jiang Yan ¹, Jing Zhang ^{1,*} and Mikhail R. Baklanov ^{1,6,7}

¹ Department of Microelectronics, North China University of Technology, Beijing 100144, China; jinming@naura.com (J.M.Z.); jiangyan@ncut.edu.cn (J.Y.); zhangj@ncut.edu.cn (J.Z.)

² Department of Physics, Mawlana Bhashani Science and Technology University, Santosh, Tangail-1902, Bangladesh; rasadphy@mbstu.ac.bd (M.R.)

³ Skobeltsyn Institute of Nuclear Physics, Lomonosov Moscow State University, 119991 Moscow, Russia; deris2002@mail.ru (D.A.S.)

⁴ Institute of Physics, University of Tartu, 50411 Tartu, Estonia

⁵ Leibniz Institute of Surface Engineering (IOM), Leipzig 04318, Germany; sergej.naumov@iom-leipzig.de (S.N.)

⁶ MIREA - Russian Technological University (RTU MIREA), Moscow 119454, Russian Federation; alexeysw@mail.ru (A.S.V.); vorotilov@live.ru (K.A.V.); baklanovmr@gmail.com (M.R.B.)

⁷ European Centre for Knowledge and Technology Transfer (EUROTEX), Brussels 1040, Belgium

* Correspondence: rasadphy@mbstu.ac.bd (M.R.); zhangj@ncut.edu.cn (J.Z.)

Abstract: UV induced photoluminescence of organosilica films with ethylene and benzene bridging groups in their matrix and terminal methyl groups on the pore wall surface is studied to reveal optically active defects and understand their origin and nature. Careful selection of the film's precursors and conditions of deposition and curing, analysis of chemical and structural properties led to the conclusion that luminescence sources are not associated with the presence of oxygen-deficient centers, as in the case in pure SiO₂. It is shown that the sources of luminescence are the carbon-containing components that are part of the low-k-matrix, as well as the carbon residues formed upon removal of the template and UV induced destruction of organosilica samples. A good correlation between the energy of the photoluminescence peaks and the chemical composition is observed. This correlation is confirmed by the results obtained by the Density Functional theory. The photoluminescence intensity increases with porosity and internal surface area. The spectra become more complicated after annealing at 400 °C, although Fourier transform infrared spectroscopy does not show these changes. The appearance of additional bands is associated with compaction of low-k matrix and segregation of template residues on the surface of the pore wall.

Keywords: low-k dielectrics; organosilica glass; interconnects; photoluminescence; oxygen deficient centers

1. Introduction

The Porous organosilica films have many different applications from catalysis, drug and gene delivery to microelectronics [1]. One of the most economically significant applications is in interconnects of Ultra large-scale integration (ULSI) devices where porous low-dielectric constant (low-k) materials are used to reduce signal propagation delay in metallization wires [2]. However, integration of porous low-k materials with metal wires faces numerous challenges, and the most important problems are related to the degradation of their dielectric properties and reliability. The most studied factors that degrade leakage current and reliability are related to structural modifications and adsorbed moisture in "plasma-damaged" low-k dielectrics and hydrocarbon

residues formed during the sacrificial porogen removal [3,4,13–15,5–12]. Photon irradiation increases the intrinsic defect density and creates trapped charges inside the low-k material, which can lead to reliability issues [16,17]. The knocking-off of atoms from the low-k material network can also occur during the ion sputtering process leading to the formation of Si vacancies such as EX centers or dangling carbon bonds, where the carbon related defects contribute to a higher leakage [18]. Furthermore, formation of surface oxygen vacancies, probably due to the removal of terminal organic groups after Ar^+ sputtering, leads to formation of sub-gap surface states at 5.0 and 7.2 eV [18]. Atomic defects such as non-bridging oxygen hole center (NBOHC) and oxygen vacancies (E'centers) have been studied with electron spin resonance (ESR) spectroscopy and the results of these studies of low-k materials are discussed and summarised in Refs. [17,19,20]. Recently, the UV induced photoluminescence (PL) of a mesoporous organosilica low-k dielectric was studied [21] and it was concluded that the formation of oxygen-deficient centers (ODCs), ODC(I) ($\equiv\text{Si}-\text{Si}\equiv$) and ODC(II) ($=\text{Si}:$) centers, similar to the observed in pure SiO_2 [22,23] can explain the leakage current mechanism studied in the Refs. [24,25]. However, it is not always easy to distinguish between the influence of atomic defects and residual carbon on the critical properties of organosilicate glass (OSG) low-k dielectrics.

So far, most defect studies have been performed with so called methyl-terminated organosilica glasses: silica like materials, where some oxygen bridging atoms in silica matrix are replaced by 2 methyl groups ($\equiv\text{Si}-\text{O}-\text{Si}\equiv \rightarrow \equiv\text{Si}-\text{CH}_3 \dots \text{CH}_3-\text{Si}\equiv$). This reduces the matrix density but makes the films sufficiently hydrophobic. These materials are mainly deposited using plasma enhanced chemical vapor deposition (PECVD) [26]. However, the need to improve the mechanical properties and reliability of low-k dielectrics stimulated extensive study of materials with different kinds of carbon bridges between silicon atoms [27–34]. The replacement of the oxygen bridge by carbon makes it possible to significantly improve the mechanical properties due to the higher bending rigidity of the $\equiv\text{Si}-\text{C}-\text{Si}\equiv$ bonds than that of the $\equiv\text{Si}-\text{O}-\text{Si}\equiv$ bonds [31]. Evaporation-induced self-assembly (EISA) [35] using carbon-bridged alkoxy silane precursors has been shown to produce periodic mesoporous organosilica (PMO) with ordered porosity and hydrocarbon bridges in the film matrix. Their properties including the thermal and chemical resistance of different carbon bridges have been extensively evaluated [36–38].

The present research aims to study the origin of ultra-violet (UV) induced PL in porous organosilica films containing various organic components. The deposited films had well-defined chemical composition and porosity. Using materials with different and controlled compositions and porosities (Figure 1), we targeted to understand the physical nature of optically and electrically active defects.

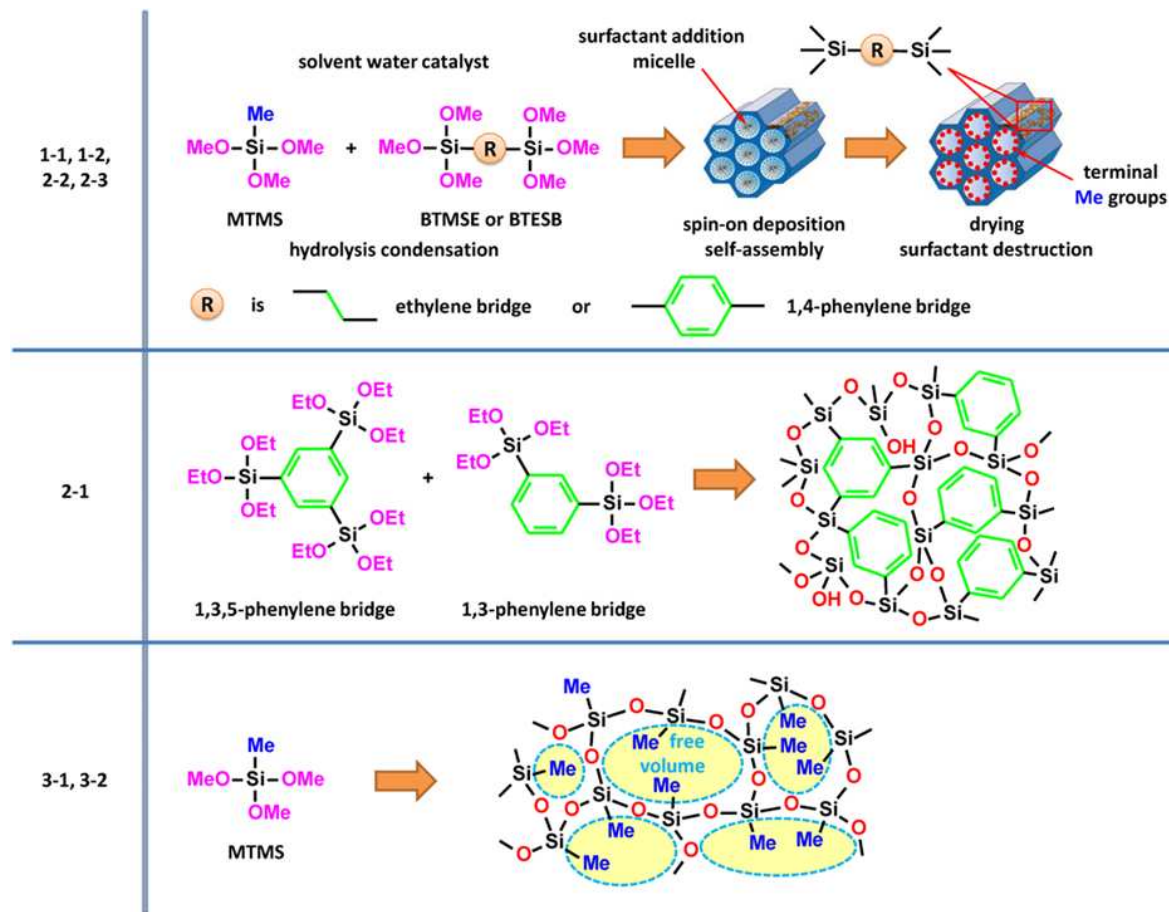


Figure 1. Schematic presentation of the samples used in this research.

Three different types of organosilica glasses are used in this research. The first type (1-1, 1-2, 2-2, 2-3) includes periodic mesoporous organosilica with ethylene and 1,4-benzene bridges in their matrix. The second type (2-1) of the films includes recently proposed “hyperconnected structure” based on 1,3,5- and 1,3-benzene bridges [33]. The third type of the films (3-1, 3-2) have a “classic” low-k structure with methyl terminal groups and random porosity [2,3]. Conditions of their preparation and properties is described in experimental part and in Supplement, and even more detailed information can be found in the cited original publications.

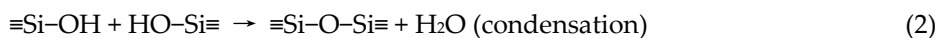
2. Materials and Methods

2.1. Material Preparation

i. The first type of samples includes ethylene bridged PMO materials (Figure 1). Precursor solutions were prepared by co-hydrolysis of alkylenealkoxysilane–1,2-bis(triethoxysilyl)methane (BTMSE) with alkylalkoxysiloxane–methyltrimethoxysilane (MTMS) under acidic conditions as described in detail in Refs. [39,40]. Due to the presence of both BTMSE and MTMS, the film contains both ethylene bridge and methyl terminal groups (Figure 1). This approach is used for low-k films preparation since the materials containing only carbon bridge do not have sufficient hydrophobicity. Conversely, materials with only terminal methyl groups have insufficiently good mechanical properties due to the reduction of matrix connectivity. All films were deposited on Si (100) wafers and film preparation is completed by a two-step annealing process: 1) soft-baking at 150 °C for 30 min on a hot plate for the solvent removal, 2) hard-baking at 400 °C during 30 min in an oven with dry air. After deposition and curing, the wafers were cut for analysis by different techniques.

To prepare the films with different porosity but the same matrix composition, the matrix solution was divided into four parts, and different amounts of Brij®30 surfactant were added and stirred. The added surfactant acts as a porogen, directing the structure forming micelle-forming structure and

interacting with the precursor. After the bulk structure was assembled, the surfactant was removed, leaving pores, or channels, embedded in the material framework. The formation of hybrid OSG films is based on the hydrolysis and condensation of MTMS and BTMSE precursors:



As deposited (AD) films contain silanol groups formed as a result of precursor hydrolysis (Reaction 1) and some unreacted methoxy ($-\text{OCH}_3$) groups from precursors. The concentration of these groups can still be significant after soft bake at 150 °C (SB) but almost not detectable after final curing at 400 °C (HB). SB films mainly reflect the non-relaxed structure determined by reactions (1) and (2). HB increases the degree of cross-linking of the organosilicate matrix with a significant improvement in the bonding structure of the Si–O–Si network [5,41]. At this stage, the matrix compaction occurs, accompanied by the segregation of unassembled porogen residues from the low-k matrix. Photoluminescence was measured from AD samples, SB and HB samples. Samples termed “as deposited (AD)” were dried at room temperature and 60–80 °C for 10 minutes. Destruction of ethylene bridge during AD and SB is not expected and these samples cannot contain ODC centers.

ii. Pure 1,4-benzene bridged films (2-2 and 2-3 in Figure 1) were deposited by using 1,4-bis(triethoxysilyl)-benzene (BTESB). The “dense” version of the films had EP measured porosity (free volume) of about 10% (1,4-BB), while the sample deposited with 30 wt% porogen had a porosity of about 29% (1,4-BB-p). In contrast to the ethylene bridged and methyl-terminated samples, the benzene bridged films had an extremely small pore size of about 0.5 nm against 3 nm in MTMS-p (3-2) samples. It also had much better mechanical properties as demonstrated in the paper [42]. Also, all the details related to the film deposition, including the curing condition and measurement procedures can be found in Ref. [42].

iii. Recently, hyperconnected structures developed by groups at IBM and Stanford University have attracted particular interest [33]. These films were deposited by using mixture of 1,3,5-tris(triethoxysilyl)benzene and 1,3-bis(triethoxysilyl)benzene as described in Refs. [43,44]. The architecture of the hyperconnected network has been achieved through the use of 1,3,5-silyl benzene precursors, where each silicon atom can be connected to the five other nearest silicon neighbours. Thus the 1,3,5-benzene bridging group structure connects each silicon atom to two others via carbon bridges that share one common Si–C bond while maintaining the ability of a silicon atom to connect with three others via Si–O–Si bonds (Figure 1b in Ref. [33]). The films with different ratio of 1,3,5- and 1,3-benzene bridges were deposited and analysed.

iv. The films containing only terminal methyl groups (3-1 and 3-2 in Figure 1) were deposited using pure MTMS precursor. The film 3-1 was deposited as a “dense” (without sacrificial porogen) and the film 3-2 by the addition of 30 wt% Brij®30 surfactant $\text{C}_{12}\text{H}_{25}(\text{OCH}_2\text{CH}_2)_4\text{OH}$. The samples deposited with porogen had an open porosity of about 33%, measured by ellipsometric porosimetry (EP) [45], while the “dense” sample had micropores with open free volume about 8% [42].

The physical properties of all deposited materials used are summarized in Table S1. All samples were thermally cured: UV light and plasma were not used for curing.

2.2. Analysis

The chemical composition of the films (1-1, 1-2, 2-1) were analyzed by Nicolet 6700 (Thermo Electron Corporation) Fourier transform infrared spectroscopy (FTIR) in the range 4000–400 cm^{-1} with a resolution of 4 cm^{-1} (64 scans) in transmission mode. The optical characteristics of the films, including thickness and refraction index (RI) were measured with a SE850 (Sentech) spectroscopic ellipsometer ($\lambda = 300\text{--}800 \text{ nm}$) using the Cauchy polynomial function. The porosity and pore size distribution of the films were characterized by atmospheric pressure EP [45]. Isopropyl alcohol (IPA) vapours (and heptane vapours in some cases) diluted with dry N_2 carrier gas in a specially designed bubbler were used as an adsorptive. The open porosity of the films is calculated as the volume of adsorbed liquid adsorbate from RI values measured during IPA adsorption using a modified Lorentz–Lorenz equation[45]:

$$\frac{n_{eff}^2 - 1}{n_{eff}^2 + 2} = V \frac{n_{ads}^2 - 1}{n_{ads}^2 + 2} + (1 - V) \frac{n_s^2 - 1}{n_s^2 + 2}, \quad (3)$$

where n_{eff} is the measured RI of the porous film when the pores are gradually filled by adsorbate at different relative pressures, n_{ads} is the RI of the liquid adsorbate, n_s is the matrix RI, and V is the volume of the condensed adsorbate. The calculation of the pore size distribution (PSD) is based on the analysis of adsorption isotherms. The analysis is based on the Kelvin equation, which describes the dependence of relative pressure (P/P_0) on meniscus curvature similar to the standard Barrett-Joyner-Halenda (BJH) procedure used in nitrogen adsorption porosimetry [46]. The size of micropores uses the Dubinin-Radushkevich approach based on Polanyi's potential theory of adsorption. EP also allows us to calculate so-called cumulative surface area. The specific surface area of each small group of pores dA_i are calculated from the corresponding pore volume and pore radius as $dA_i = dV_i/r_i$ (for cylindrical pores). A value of the cumulative surface area is obtained by assuming the values of dA_i over the whole pore system.

UV induced luminescence of samples with ethylene bridge (1-1 and 1-2) and 1,3,5- and 1,3-benzene bridge (2-1) samples were measured on a JASCO FP-8300 spectrofluorometer using a continuous output Xe arc lamp with shielded lamp housing (150 W) and holographic concave grating in a modified Rowland mount monochromator. The radio-photometer system using monochromatic light was used to monitor the output intensity of the Xe lamp. The samples were mounted in a standard 10 mm rectangular cell holder SCE-846/D061161450 provided by JASCO. The wavelength accuracy and maximum resolution is 1 nm. The excitation and emission spectra are in the range in the energy range from 6.2 to 1.65 eV and the slit width is 5 nm–5 nm. Measurements were performed at room temperature and fully controlled using a Spectra Manager. The excitation and emission bandwidth were 5 nm with a scan speed of 1000 nm/min.

The methyl-terminated (3-1, 3-2) and 1,4-benzene bridged samples (2-2 and 2-2) were measured at excitation energies from 6 to 10 eV using a different system. Luminescence and luminescence excitation spectra were measured using the photoluminescence end station of the FinEstBeAMS beamline at the 1.5 GeV storage ring of the MAX IV synchrotron facility [47]. The luminescence excitation spectra were measured with a spectral resolution of no less than 4 meV using fused silica and MgF_2 optical filters in the energy range 4.5–7.0 eV and 6.5–11 eV, respectively. The samples were placed into a closed-cycle helium cryostat from ARS, equipped with a LakeShore 325 temperature controller and the measurement temperature was equal to 7 K. Before measurements, the samples were degassed at 350 K in a vacuum of 10^{-9} mbar. An excitation flux curve obtained using a factory calibrated AXUV-100G diode (OptoDiode Corp, USA) was used to correct the excitation spectra. The luminescence spectra were recorded using a fiber-coupled Andor Shamrock SR-303i (Andor Technology Ltd, Belfast, UK) spectrometer equipped with a photon counting head Hamamatsu H8259-01. The luminescence spectra were corrected for the spectral sensitivity of the registration channel.

It is necessary to mention that all other characteristics of the films like dielectric constant, mechanical properties, surface roughness, pore ordering, plasma and VUV properties have also been studied by using different instrumentations. These data are not discussed in this paper but can be found in the references [36–40,48,49].

2.3. Calculation of the Energy Diagram of UV Induced Processes

Density Functional Theory (DFT) calculations were carried out systematically employing the PBE0 density functional [50–52]. The way in which the PBE0 functional is derived and the lack of empirical parameters fitted to specific properties make the PBE0 model a widely applicable method for quantum chemical calculations. The molecular geometries, energies and electronic structure of the molecules were studied at the PBE0/6-31G** level of theory, as implemented in the Jaguar 9.6 program [53]. This computational model was already successfully used for calculations in our previous work [54,55]. Frequency calculations were performed at the same level of theory to obtain the total enthalpy (H) and Gibbs free energy (G) at a standard temperature of 298.15 K using unscaled frequencies. The reaction enthalpies (DH) and Gibbs free energies of the reaction (DG) of studied

molecules were calculated as the difference of the calculated H and G between the reactants and products, respectively. The excited states and electronic transition spectra were calculated in the gas phase using the time dependent (TD) DFT method [56] at the PBE0-D3/6-31G** level of theory. The excited states calculations were performed using the Full Linear Response (FLR) approximation [57] as implemented in the Jaguar 9.6 program.

3. Results

3.1. Ethylene Bridged PMO [39,40]

FTIR spectra of fully cured ethylene bridged PMO films (1-1, 1-2) are shown in Figure 2. The absorption band at 1250–1000 cm⁻¹ corresponds to Si–O stretching modes. The soft baked (SB) at 150 °C films show presence of hydroxyl and silanol groups (O–H, Si–OH) at 3700–3100 cm⁻¹ and C=O group at 1750 cm⁻¹ which are removed after hard bake (HB). The Si–OH concentration in SB films is higher in the films deposited without or with a small concentration of porogen. The possible reason is that the remaining porogen makes the films more hydrophobic. It can be seen that SB films still contain a significant amount of C–H_x (x = 2 or 3) groups in the wavenumber range (3000–2800 cm⁻¹) and C–H (1460 cm⁻¹). They mainly originated from the template (Brij®30) and this is the reason why their concentration increases with initial porogen concentration (Figure 2b). HB reduces those group concentrations (Figure 2d). The presence of Si–CH₃ terminal groups can be seen from the peak at ~1275 cm⁻¹ and Si–CH₃ groups also contribute to the intensity of hydrocarbon peaks at ~2970 and ~2920 cm⁻¹.

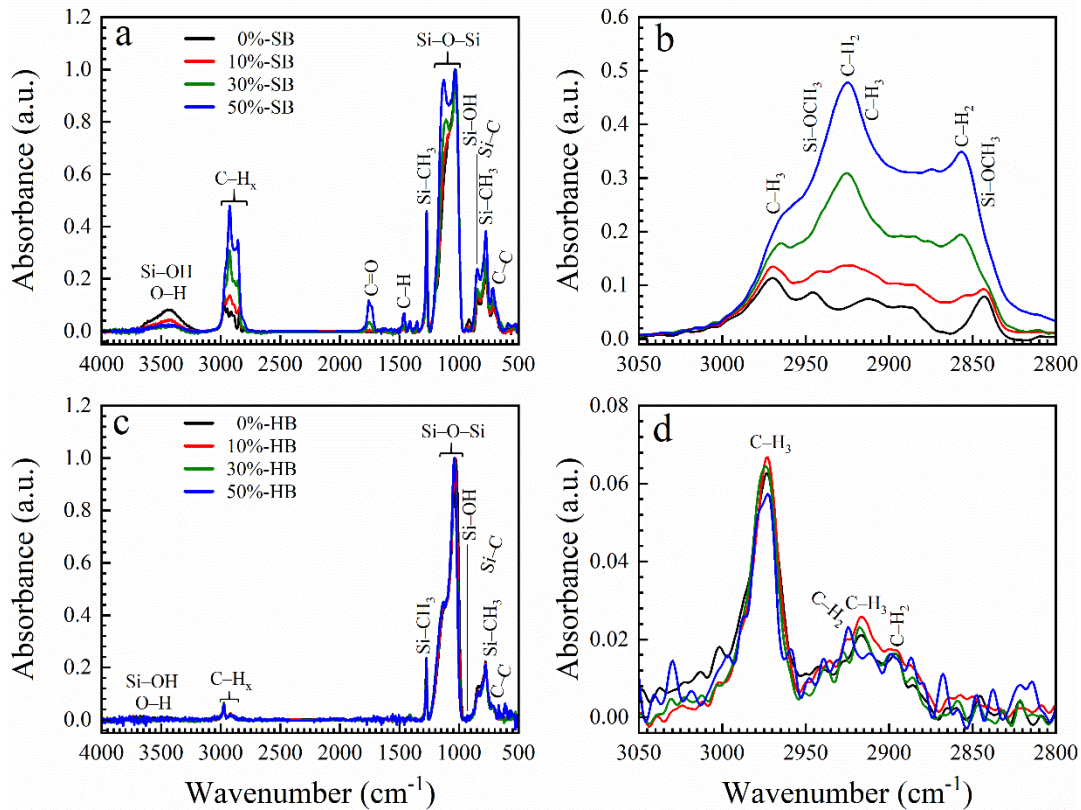


Figure 2. FTIR spectra of OSG low-k samples deposited with BTMSE/MTMS precursor ratio of 25/75 and different porogen concentrations (0–50 wt%) after soft bake at 150 °C (SB) in the air (a,b) and hard bake at 400 °C (HB) in the air (c,d). FTIR spectra of the samples deposited with a BMTSE/MTMS ratio of 47/53 are qualitatively similar.

Figure 3 shows adsorption-desorption isotherms of heptane vapors measured by EP. The isotherms of all samples deposited with 0–30 wt% template do not have a hysteresis loop, indicating that the pores are cylindrical in shape. However, the samples deposited with 50 wt% template have

pronounced hysteresis loops typical for the formation of internal voids leading to "ink-bottle" like effects in isotherms [58].

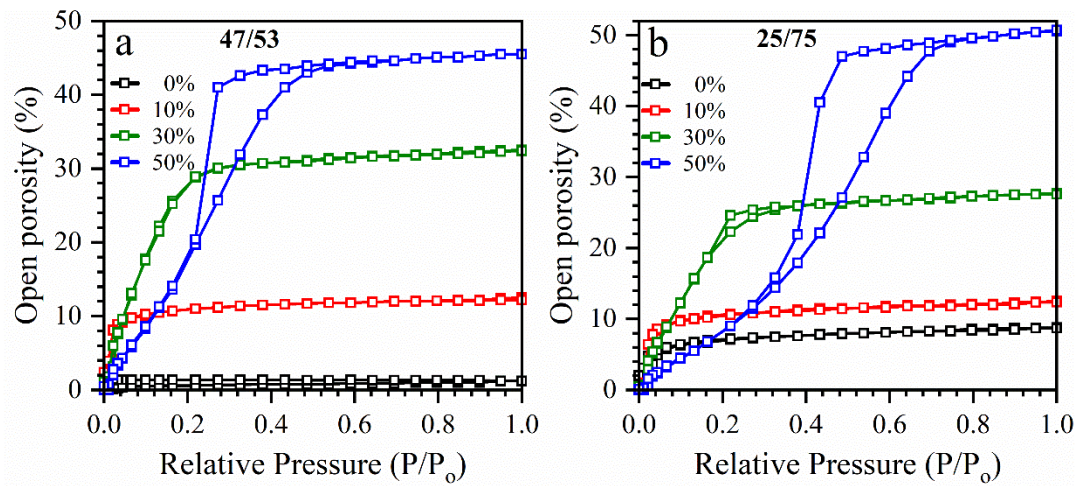


Figure 3. Adsorption-desorption isotherms of heptane vapor in the OSG low-k films deposited with BMTSE/MTMS ratio of 47/53 (a) and 25/75 (b) and different porogen concentrations (0–50 wt%).

Clear difference can be seen between the samples deposited with BMTSE/MTMS ratios 47/53 and 25/75. The isotherms in samples with a BMTSE/MTMS ratio of 25/75 have critical slopes at higher relative pressures P/P_0 , indicating a larger pore size. They also have higher porosity than the samples deposited with BMTSE/MTMS ratio 47/53 and this difference becomes even pronounced in the samples deposited with 30 and 50 wt% of template (Figure 3). A reasonable explanation is that ethylene bridge increases the stiffness of the matrix and hinders agglomeration of template molecules during the matrix formation. However, no principal differences in photoluminescence spectra are observed between 47/53 and 25/75 samples (Figure 4).

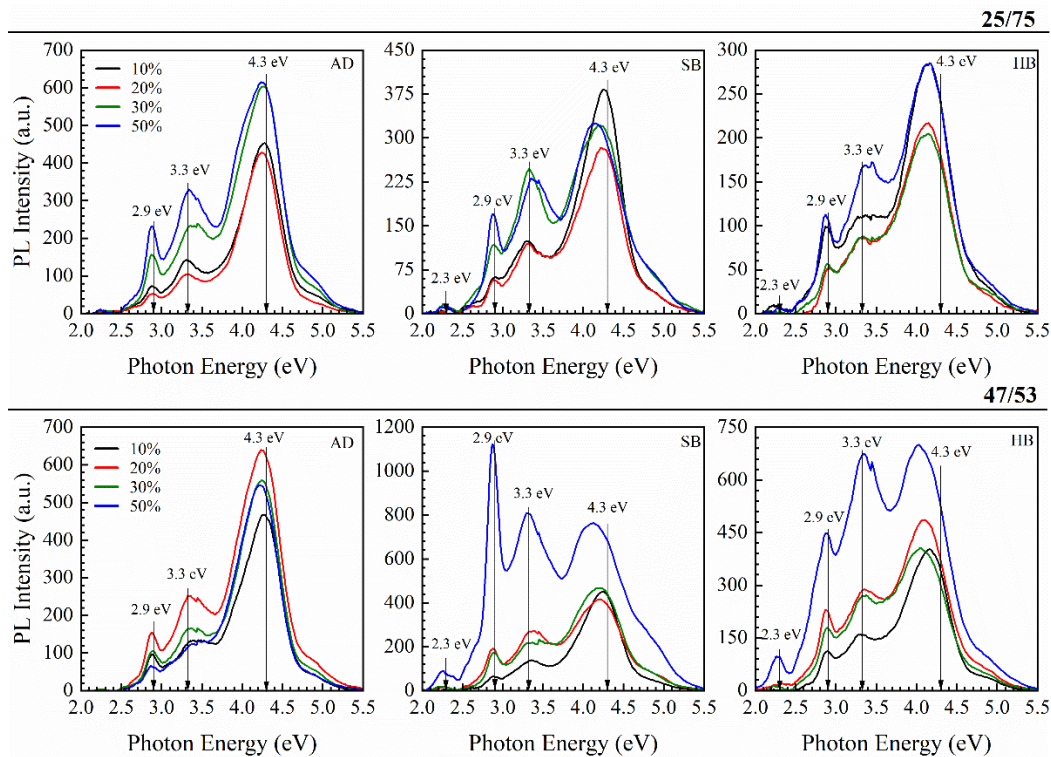


Figure 4. UV induced room temperature luminescence of PMO low-k films containing both methyl terminal and ethylene bridging groups. The films have different porosity and they were cured in air. The samples deposited with BMTSE/MTMS ratio of 25/75 (top line) and 47/53 (bottom line) with

different porogen concentrations (10–50 wt%) as deposited (AD), after soft bake at 150 °C (SB) in air and hard bake at 400 °C (HB) in air, upon excitation with light of 6.2 eV. The data are reproduced from the paper “Effect of methyl terminal and ethylene bridging groups on porous organosilicate glass films: FTIR, ellipsometric porosimetry, luminescence dataset” by Md Rasadujjaman, J. Zhang, K. P. Mogilnikov, A. S. Vishnevskiy, J. Zhang, M. R. Baklanov (Data in Brief 35 (2021) 106895) with granted permission from ELSEVIER.

The measured luminescence spectra clearly show three peaks located near 4.3, 3.3, and 2.9 eV. The position of these peaks is the same as in the paper [21], where the films of the same series (BTMSE/MTMS = 25/75 ratio, porosity 30%) were studied upon excitation by synchrotron radiation. The only differences relate to the relative intensities of the peaks but it is likely a sample storage issue. The peaks interpretation in the Ref. [21] is based on information reported for SiO_2 . According to [22,23], the peaks at 4.3 and 3.2 eV are often observed in SiO_2 and can correspond to ODC(I) defects ($=\text{Si}-\text{Si}=$), and the peak at 2.9 eV was interpreted as emission from ODC(II) defect ($-\text{Si}:-$).

In our case, the positions of 2.9 and 3.2 eV peaks are constant in all three types (AD, SB, HB) of films but the position of 4.3 eV is changing during the curing. This peak corresponds to 4.3 eV in as deposited (AD) films, then decreases to ~4 eV in SB samples at 150 °C and HB samples at 400 °C. This shift is too significant to be assigned to only ODC(I). The shift of the 4.3 eV peak in principle can be interpreted as the result of the formation of additional peaks at $E < 4$ eV, which can be assigned to specific carbon containing residues [59–63]. In the general case, the formation of ($=\text{Si}-\text{Si}=$) type defects should occur due to the destruction of certain bonds of Si atoms. It can be assumed that they can be formed due to the destruction of carbon bridges, which have the lowest thermal stability in this system. However, the $-\text{Si}-(\text{CH}_2)_2-\text{Si}-$ bonds are sufficiently stable and certainly cannot be destructed in AD and SB films ($T < 200$ °C). Therefore, the assignment of this peak to ODC(I) (Ref. [21]) is doubtful. The peak at 2.9 eV in BTMSE/MTMS = 47/53 sample increases drastically during SB and remains quite high after HB. It also generates doubt on the assignment to ODC(II) since, according to the Ref. [22], ODC(I) is typically much more abundant than ODC(II) because ODC(II) might be a product of a partial transformation of ODC(I).

3.1.1. Effect of Storage and ICP Oxygen Plasma

The evolution of PL intensity in a sample with a BTMSE/MTMS ratio of 45/53 (HB) is shown after storage in the air in a clean room environment (Figure 5a). PL intensity gradually increased every week and finally increased ~10 times after 1 month. Figure 5b shows that the first PL measurement of a sample stored after one month reduces the PL intensity by about 10%. The following measurements one after another with a break of a few minutes slightly reduce the intensity.

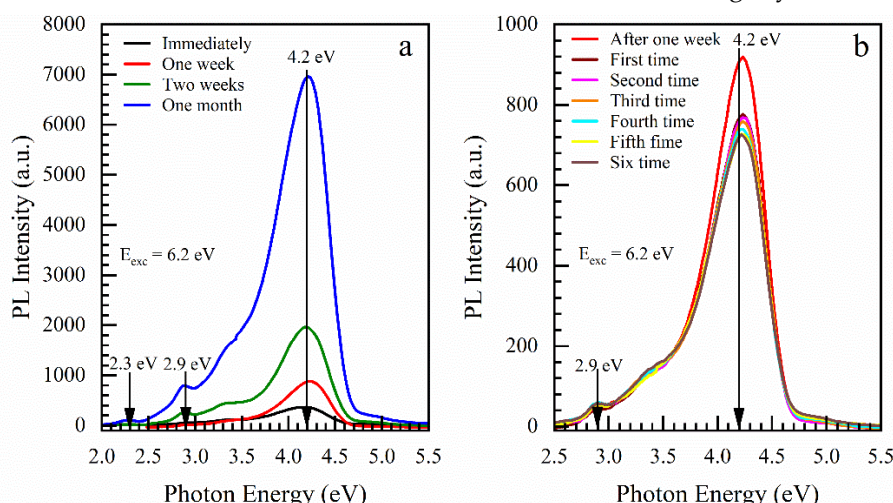


Figure 5. (a) Effect of storage in a clean room environment on the PL intensity for the OSG films deposited with a BTMSE/MTMS ratio of 47/53 and (b) PL measurements one after the another with a break of a few minutes.

The corresponding change in chemical composition during sample storage can be seen in FTIR spectra (Figure 6a). Air storage accumulates hydrocarbon residues from the clean room environment. Such effect is well known for porous low-k materials: capillary forces enhance adsorption and condensation of hydrocarbons and other residues. The observed decrease in PL intensity in air stored samples after the first measurement can be related to UV induced desorption of a part of the carbon residue.

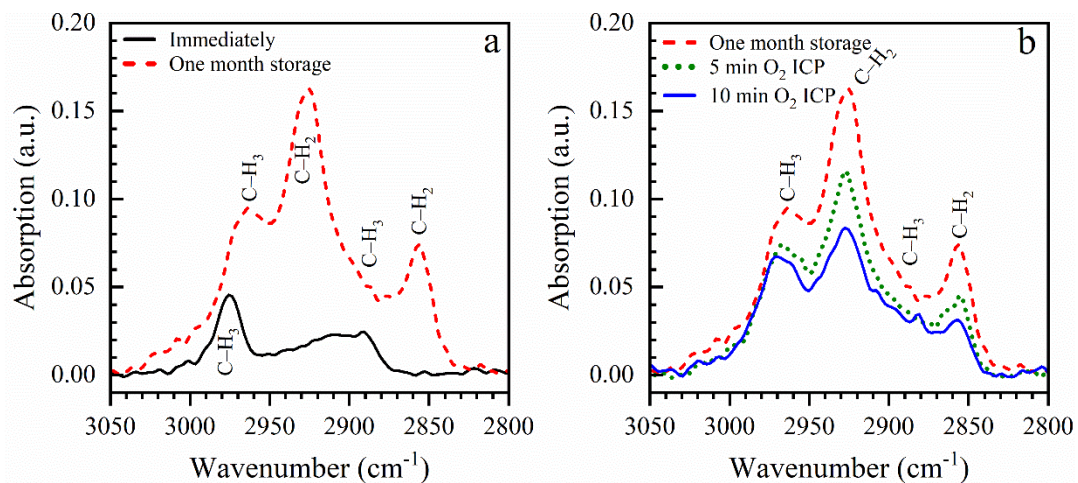


Figure 6. Accumulation of hydrocarbon residues from a clean room environment (a) and removal of these residues by ICP oxygen plasma (b).

When this sample is exposed to soft oxygen inductively coupled (ICP) plasma (Figure 6b), the concentration of the hydrocarbon containing species is reduced. At the same time, also some loss of $\text{Si}-\text{CH}_3$ groups and hydrophilization is also observed (see supplement Figure S1). Reducing the carbon concentration leads to a reduction in PL intensity at 4.2 eV (Figure 7). The change happening in PL intensity during storage and exposure to O_2 ICP plasma clearly shows that the intensity of the peak near 4.1–4.2 eV is related to hydrocarbon residues accumulated during the template removal (pristine sample) and storage in air. PL of hydrogenated carbon has been extensively studied in the past. According to these publications, in addition to the well-known broad PL bands at 2.1–2.33, 2.85–2.92 eV and 3.17–3.22, other peaks located at 3.64–3.70, , 3.93–4.01 and 4.34–4.56 eV in the UV region can also be found [64]. The observed change in PL spectra in the carbon rich films deposited with high template concentration (50 wt%) and high BTMSE/MTMS ratio (Figure 4) and the increase in intensity of certain peaks during thermal curing and exposure in O_2 ICP plasma most probably reflects the modification of carbon containing components of the films studied.

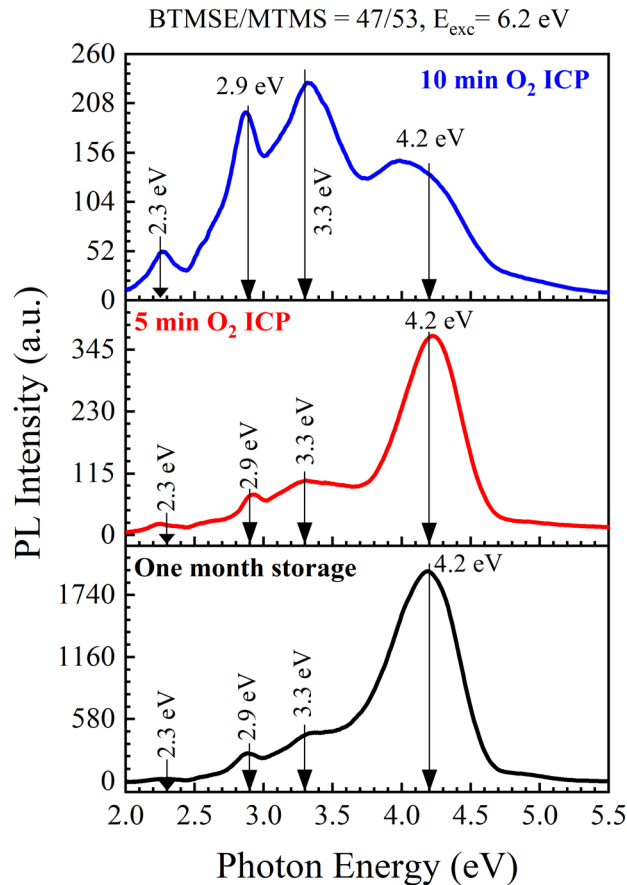


Figure 7. Reduction of 4.2 eV PL intensity during exposure to ICP oxygen plasma. The excitation energy of the photon was 6.2 eV.

3.2. Benzene Bridged Organosilica Films

3.2.1. 1,3,5- and 1,3-benzene Bridged Films [33,43,44]

The films with different molar ratios of 1,3,5-tris(trimethoxysilyl)benzene to 1,3-bis(trimethoxysilyl)benzene bridging organic groups (1:3 and 1:7) were spin-on deposited, followed by a soft bake in air at 150 °C (SB) and hard bake in air at 400 °C (HB). The concentrations of the non-ionic template (Brij®30) were varied from 0 to 41 wt%. The chemical composition of the matrix of the films was evaluated and discussed, as well as refractive indices, mechanical properties, k-values, porosity and pore structure.[43,44] The films containing benzene bridging groups keep the pore size constant and equal to 0.81 nm while changing their porosity from 0 to 30%. The films containing a benzene bridge have a higher a Young's modulus than plasma-enhanced chemical vapor deposition (PECVD) methyl-terminated low-k films with the same porosity [33]. The fabricated films show good stability after a long time of storage. FTIR spectra and porosity data generated by ellipsometric porosimetry are presented in the SI as Figures S2 and S3.

Figure 8 shows photoluminescence spectra for 1:3 and 1:7 samples. This means that the 1:3 sample has a 2.3 times higher concentration of 1,3,5-benzene rings than the 1:7 sample. The most important difference from ethylene bridged films is that AD and SB films contain only 1 pronounced peak at around 3.9 eV. Looking at the PL spectra of samples AD and SB, one can conclude that the intensity increases with increasing porosity. The PL spectra of HB films are becoming more complicated and new peaks near 2.3, 2.9 and 4.85 eV are observed.

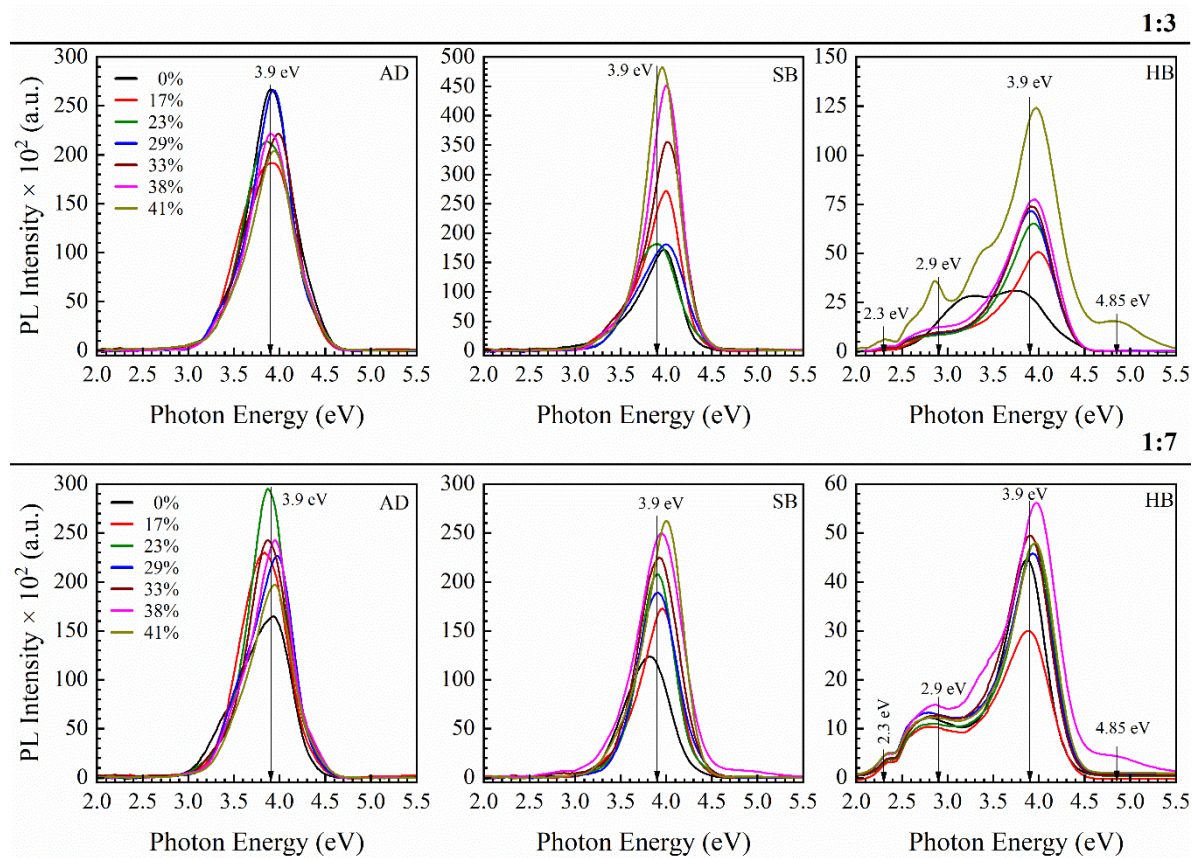


Figure 8. Photoluminescence spectra of OSG films containing 1,3,5- and 1,3-benzene bridges (samples 2-1 in Figure 1) and different porosity, upon excitation with light of 6.2 eV. The porogen concentration was varied from 0 to 41 wt%. The ratio of 1,3,5- and 1,3-benzene bridges is equal to 1:3 in the top line and 1:7 on the bottom lines. AD, SB and HB have the same meaning as in the samples with ethylene bridge (Figure 4).

3.2.2. 1,4 benzene Bridged Films [42]

Two different types of 1,4-benzene bridged films were prepared. The first one (1,4-BB) was prepared from pure BTESB (1,4-bis(triethoxysilyl)-benzene) without porogen and without methyl terminal precursors and had an intrinsic porosity of about 10%. The second type of film (1,4-BB-p) was prepared also with BTESB but 30 wt% of porogen was added into the precursor. As a result, the film has 30% EP measured porosity. FTIR and EP data can be found in the SI, as Figures S4 and S5. All of these samples were fully cured: they went through the SB and HB processes. PL spectra of 1,4-BB film was measured at the photoluminescence station of the FinEstBeAMS beamline at the 1.5 GeV storage ring of the MAX IV synchrotron facility [47]. The measurements were done at 7K after outgassing in ultrahigh vacuum (10^{-9} mbar) at 350K. PL spectra have clearly defined peak at 3.67 eV (at excitation by 5.6 eV) and 3.69 eV (at excitation by 7.3 eV) (Figure 9). Deconvolution shows the presence of 2.86 eV peak and also there are traceable emissions with wavelengths 2.24 and 4.2 eV. The introduction of porogen changes the main emission to 3.76–3.78 eV and presence of 4.20 eV is becoming more pronounced (Figure 9b). It supports our previous conclusion that emission at 3.9–4.2 eV is related to hydrocarbon residue: removal of porogen always tends to leave a certain amount of porogen residue [5–7]. The similarity of the PL spectra of these samples with the PL spectra of HB samples with 1,3,5/1,3-benzene bridges (Figure 8) shows that the key role is played by the presence of the benzene bridge rather than the type of their bond with Si atoms.

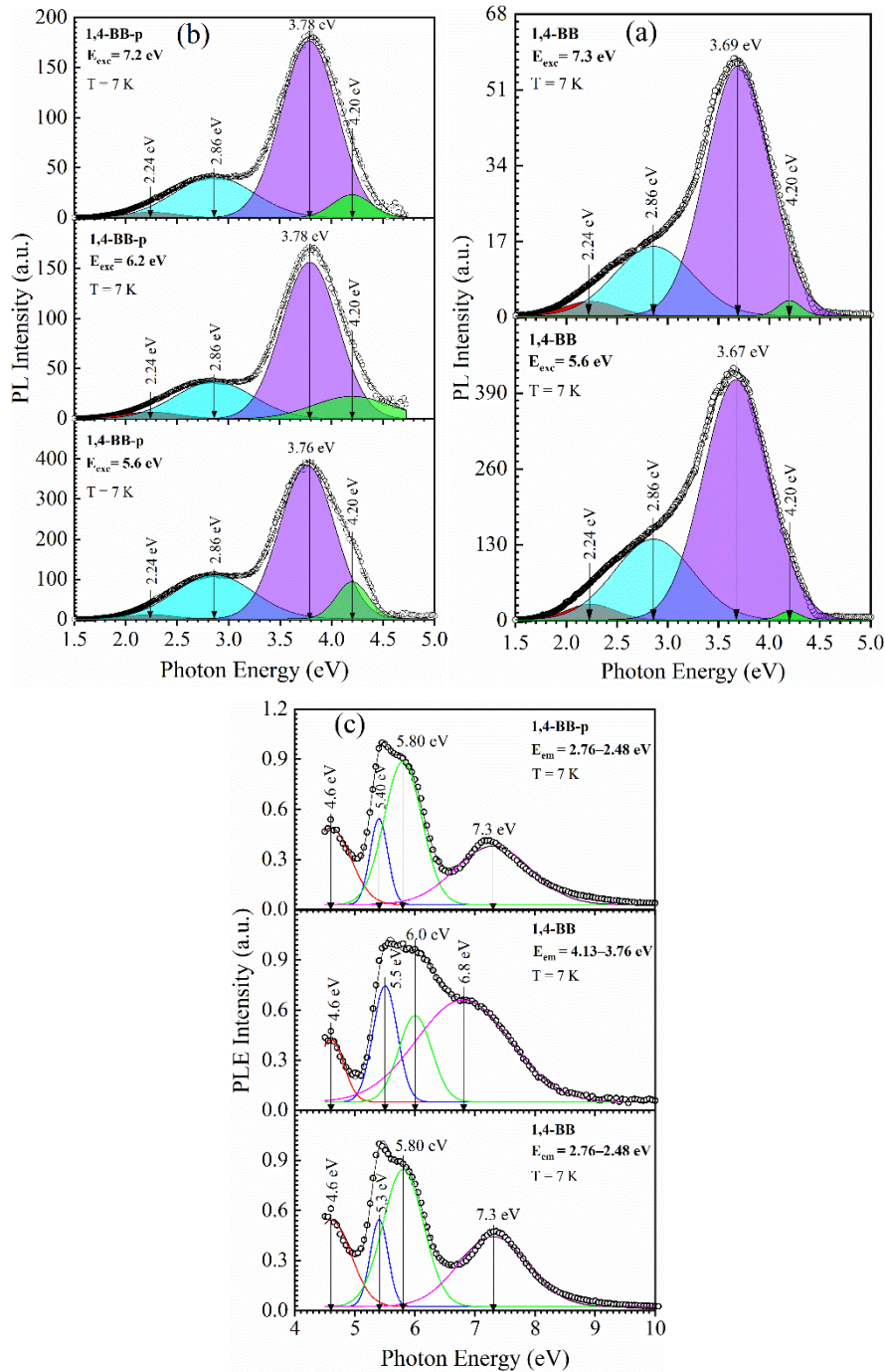


Figure 9. PL spectra of non-porous hard baked OSG film with 1,4-benzene (1,4-BB) bridge upon excitation by 5.6 and 7.3 eV photons (a) and porous films with 1,4-benzene bridge (1,4-BB-p) upon excitation by 5.6, 6.2 and 7.2 eV (b) and PL excitation spectra for 1,4-BB film upon detection 2.76–2.48 eV and 4.13–3.76 eV and for 1,4-BB-p film upon detection 2.76–2.48 eV (c).

3.3. Methyl-Terminated Organosilica Films [65]

The films with only methyl terminal groups were fabricated using pure MTMS to prepare dense films and also with 30 wt% added porogen (MTMS-p). All of these samples were fully cured: they went through the SB and HB processes. FTIR spectra are presented in the SI as Figure S6. The measured porosities were equal to 7.5% and 33.1% (SI, Figure S7). The PL measurements also were done on the system used for 1,4-BB films. MTMS films at 7.0 eV photoluminescence excitation (PLE) showed only one peak with emission at 2.83 eV (Figure 10). Excitation by UV light with an energy 6.2 eV gave an additional peak at 4.35 eV. The last peak became much more pronounced in the films

prepared with a porogen, which also supports our previous conclusion that this peak is related to the porogen residue.

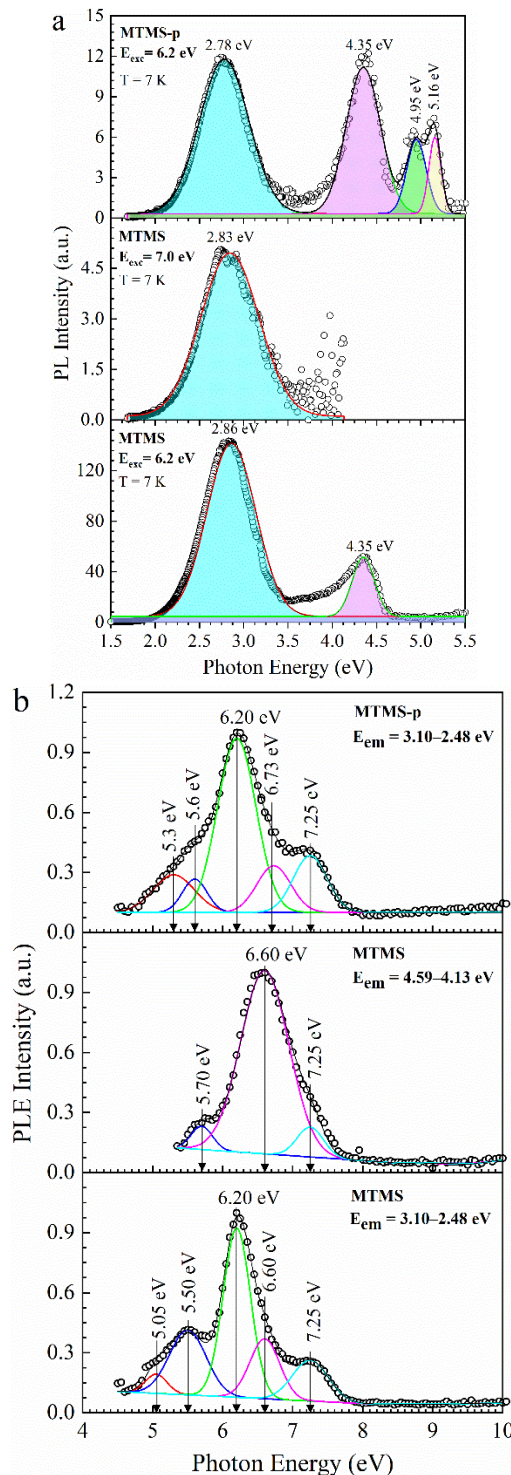


Figure 10. PL spectra of non-porous hard baked OSG film with methyl terminal group (MTMS) upon excitation by 6.2 and 7.0 eV photons and porous methyl-terminated film (MTMS-p) upon excitation by 6.2 eV (a) and PL excitation spectra of MTMS films upon detection 3.10–2.48 and 4.59–4.13 eV and MTMS-p films upon detection 3.10–2.48 eV (b).

4. Discussion

The presented results allow us to discuss the origin and nature of the observed luminescence bands. The main results are summarized in Table 1. A clear correlation of PL bands with types of organic groups is observed. 1,4-benzene bridged films (2-2) show the presence of 3.68 and 3.78 eV PL

peaks. Similar emissions at 3.9 eV have demonstrated the films containing both 1,3,5- and 1,3-benzene bridges. It suggests that these emission bands are related to benzene bridges. However, HB (400 °C) films show the appearance of small intensity PL peaks near 2.9 and 4.2 eV. It is reasonable to assume that the appearance of these peaks is associated with the compaction of the film matrix, which occurs during calcination at 400 °C and initiates the segregation of unassembled porogen fragments and other residues from the low-k matrix to the surface of the pore walls [5,41].

The samples with only terminal methyl groups show a PL band at 2.8–2.9 eV. Dense MTMS films only show the presence of this peak when PL is excited by 7.0 eV photons, but also have a small peak at 4.2 eV when PL is excited by 6.2 eV photons. The porous MTMS-p films deposited with porogen show an increase in relative intensity of 4.25 eV peak compared to dense materials. The peaks with even higher energy are observed in this sample. An important observation (Table 1) is that all samples deposited with porogen have a strong peak at 4.2–4.3 eV and this support our conclusion (Section 2.1) that it is related to porogen residue and other hydrocarbon residues.

Table 1. General characteristics of used OSG films and PL energy as a function of the carbon groups. For example, peaks at 3.78–3.9 eV are only observed in films with benzene bridges, so they can be attributed to the benzene bridge. A similar approach is used for other groups. The brackets show the low intensity peaks, which appear mainly after HB.

Sample number	Sample ID	Terminal group (-CH ₃)	Bridging group	Porogen	Characteristics PL peaks (eV)			
1-1	BTMSE/MTMS=47/53	YES	Ethylene	YES	-	3.3	2.9	4.2
1-2	BTMSE/MTMS=25/75	YES	Ethylene	YES	-	3.3	2.9	4.2
2-1	1,3,5/1,3-BB	NO	Benzene	YES	3.9	-	(2.90)	(4.85)
2-2	1,4-BB	NO	Benzene	NO	3.68	-	(2.86)	-
2-3	1,4-BB-p	NO	Benzene	YES	3.78	-	(2.86)	4.2
3-1	MTMS	YES	NO	NO	-	-	2.85	(4.35)
3-2	MTMS-p	YES	NO	YES	-	-	2.78	4.35
Assignment of PL peaks					Benzene bridge	Ethylene bridge	-CH ₃ termina	C-H _x
					1			

Ethylene bridged samples give emissions at 2.9, 3.3 and 4.2 eV. We already showed that PL peaks at 2.9 and 4.2 eV correspond to methyl terminal groups that are present in these films and porogen residues because the sample was deposited with a porogen. Therefore, the 3.3 eV peak reflects the presence of an ethylene bridge.

4.1. Diagrams of the Energy Levels Calculated by Using Density Functional Theory

Figure 11 shows energy level (Jablonski) diagrams calculated for model molecules reflecting the studied materials.

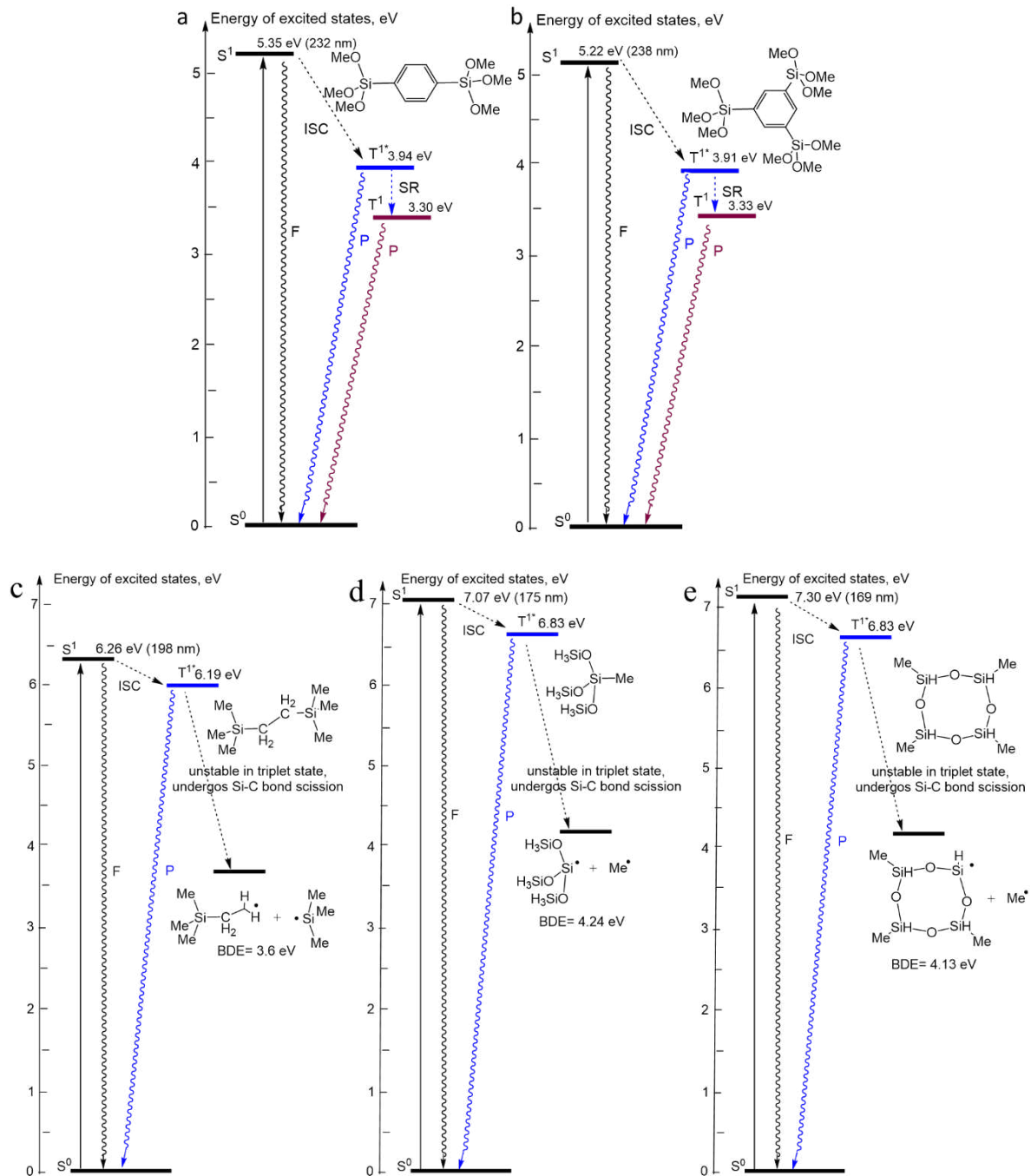


Figure 11. Calculated Jablonski diagram for model molecules containing: 1,4-benzene bridge (a), 1,3,5-benzene bridge (b), ethylene bridges (c), methyl-terminated (d,e). (F) is fluorescence, (P) is phosphorescence, ISC – intersystem crossing, SR – structural relaxation.

Figure 11a,b show the energy levels for 1,4-benzene and 1,3,5-benzene bridges. After excitation to the first excited singlet S^1 state, the molecule undergoes ISC to the excited triplet T_1^* state. The T_1^* state undergoes further structural relaxation to a more stable T_1 state due to the adjustment of molecular geometry to change the electron distribution upon excitation. Due to the large energy gap between ground S^0 and excited S^1 states, the deactivation of energy from the S^1 state may be observed by fluorescence. Otherwise, if ISC occurs, deactivation of energy through phosphorescence of both T_1^* and T_1 can be expected. Interestingly, the energy levels of all transitions in 1,4-benzene and 1,3,5-benzene bridges are very similar despite the difference bond structure. UV induced excitation initiating the singlet-singlet (S^0-S^1) transition has energies of 5.35 and 5.22 eV, which is very close to the maximum PLE energy of 5.4–5.5 eV measured for 1,4-benzene bridged OSG materials. (Figure

9c). The energy of the PL photons measured for these films was equal to 3.7 ± 0.1 eV and 3.9 eV for 1,4- and 1,3,5-benzene bridged OSG, respectively. The calculated energies for the triplet – singlet ($T_1^* - S_0$) transition have very close values equal to 3.94 and 3.91 eV. Taking into account that model molecules were used for calculations, one can conclude that the agreement between the calculated and measured PL and PLE energies is perfect. Therefore, the energy diagrams, presented in Figure 11(a,b) most likely correctly reflect the electronic transitions leading to PL.

Figure 11c shows the energy diagram for a molecule having both ethylene bridge and methyl terminal groups. After excitation to the first excited singlet S_1 state, molecules undergo ISC into the excited triplet T_1^* state. However, the T_1^* state is very unstable due to the high energy and undergo Si–O bond cleavage during optimization instead of relaxing into a more stable T_1 state. Due to the large energy gap between ground S_0 and excited S_1 states, deactivation of the energy from the S_1 state through fluorescence may be observed. Otherwise, if ISC into T_1^* state occurs, deactivation of the energy from T_1^* through phosphorescence may be expected. The calculated energy for the singlet-singlet ($S_0 - S_1$) transition for this molecule (6.26 eV) is quite close to the measured PLE energy for the sample 1-2 (BTMSE/MTMS 47/53) equal to 6.2 eV (Figure S8). However, we do not observe the emission of 6.19 eV corresponding to transition $T_1^* - S_0$. Moreover, after relaxation of T_1^* to T_1 state this molecule dissociates forming the radicals shown in Figure 11c. Nevertheless, the bond dissociation energy (BDE) is equal to 3.6 eV, which is close to PL observed with this compound ~ 3.3 eV. Simulation by Density Functional theory makes this radiative transition doubtful because of energetically preferential molecular destruction from the triplet state. It can be assumed that the destruction of these molecules occurs in parallel with UV radiation, and therefore the intensity of the characteristic 3.3 eV emission in the films with an ethylene bridge has a relatively low intensity (Figure 4).

Figure 11d,e show the energy diagrams for two different molecular structures representing methyl-terminated OSG materials. The first one reflects a model SiO_2 -like structure where one Si bond is terminated by the methyl radical. In the second structure, we selected tetramethylcyclotetrasiloxane as a model to take into account the possibility of the second (hydrogen) terminal group to be bonded to silicon. However, the energy diagrams in these 2 cases were very similar: 7.07 eV for $S_0 - S_1$ transition, and 6.83 eV for the T_1^* state. Only a small difference can be seen in BDE energy: 4.24 eV and 4.13 eV, respectively. It is obvious that the calculated values are quite different than the measured ones (6.2 eV for PLE and 2.8 eV for PL) although the PLE spectrum contains a band 7.25 eV able to provide $S_0 - S_1$ transition in these molecules. The most important feature is that according to DFT calculations, molecules in the T_1^* state become unstable and dissociate to form radicals, as shown in Figure 11(d,e). The most reasonable assumption that can explain the observed PL bands 2.78 eV in samples 3-1 and 3-2, and also PL bands 2.9 eV in samples 1-1 and 1.2 is PL of dissociation by-products. This mechanism needs additional study. However, PL measurements of the MTMS samples were carried out at 7K, while the DFT calculations correspond to room temperature. Our estimations showed that temperature has little impact on BDE, while the change in the Gibbs free energy of the reaction is significant. The dissociation of the $\text{Si}-\text{CH}_3$ bond in S_0 ground state $\text{DG}(298\text{K}) = 78$ kcal/mol and $\text{DG}(7\text{K}) = 90$ kcal/mol. For dissociation from the triplet state $\text{DG}(298\text{K}) = -104$ kcal/mol and $\text{DG}(7\text{K}) = -86$ kcal/mol. Therefore, the probability of the $\text{Si}-\text{CH}_3$ dissociation reaction at 7K is much lower and therefore parallel UV emission can also be expected. Similar phenomena were reported in the papers [66,67]. The calculated energy of emission is about 4.2 eV, which overlaps with the peak attributable to carbon residue radiation. For this reason, these peaks are observed in all samples deposited with porogen and containing CH_3 terminal groups.

Therefore, the characteristic PL emission of mesoporous organosilica films corresponds to the introduced carbon fragments. Most probably they do not include emission from oxygen deficient centers (ODC) as it was concluded in the recent publication [21]. This conclusion is based on our sample preparation strategy: the samples were not exposed to high-energy impacts capable of generating oxygen vacancies (no UV curing, no exposure to ion and plasma radiations). The curing temperature was not higher than 430°C and it is too low for formation of oxygen deficient centres.[32] It is necessary to mention that our conclusion is consistent with the results of the ESR study of different low-k materials [17,32,68,69]. The carbon dangling bond signal at characteristic $g \approx 2.003$ has

been reported in many studies addressing a broad variety of low-k dielectrics. These references can be found in Review paper [32] under numbers (306, 307, 316–321) and some others. Presence of Si vacancies like EX centers or dangling carbon bonds, where the carbon related defects contribute to a higher leakage. The presence of carbon in the film in various forms ranging from the terminal and bridging carbon groups to clusters of elemental carbon originating from porogen or template residuals can give rise to deep energy levels in the insulator bandgap causing low-field leakage currents [6,7,70].

Finally, similar conclusions were drawn based on the results of studying the PL in SiC_xO_y films deposited using thermal CVD [69]. The films deposited in this way should have similar properties to our MTMS (3-1, 3-2) films containing random porosity and methyl terminal groups. Using a parallel study of PL and ESR, authors concluded that typical structural defects in oxides, e.g., Si-related neutral oxygen vacancies or non-bridging oxygen hole centers cannot be considered as the dominant mechanism for white luminescence from SiC_xO_y . It was concluded that PL from SiC_xO_y thin films can result from the generation of carriers due to electronic transitions associated with the C–Si/C–Si–O bonds during optical absorption, followed by recombination of these carriers between energy bands and in their tail states associated with Si–O–C/Si–C bonds. Although the detailed mechanism may differ from ours, the key importance of the Si–C and Si–O–C bonds is also emphasized.

5. Conclusions

The UV induced photoluminescence of organosilica films with various combinations of ethylene and benzene bridging groups in their matrix and terminal methyl groups on the pore wall surface was studied to reveal optically active defects and understand their origin and nature. Careful selection of the films precursors and conditions of deposition and curing excluding breakage of chemical bonds, and analysis of chemical and structural properties led to the conclusion that luminescence sources are not associated with the presence of oxygen-deficient centers, as in the case in pure SiO_2 , and has also been predicted for low-k organosilica films [21–23]. It is shown that the sources of luminescence are the carbon-containing components that are part of the low-k matrix (3 different types of benzene bridges), as well as the carbon residues formed upon removal of the template and destruction of organosilica samples containing ethylene bridge and methyl terminal groups. A fairly good correlation between the energy of the photoluminescence peaks and the chemical composition is observed (Table 1). This correlation is also confirmed by the results of density functional theory calculations. The spectra are becoming more complicated after annealing at 400 °C, although Fourier transform infrared spectroscopy does not show these changes. The appearance of new peaks after annealing at 400 °C is associated with the segregation of hydrocarbon residues from the low-k matrix on the pore wall surface [5,41]. Therefore, photoluminescence spectroscopy can potentially be used as effective instrumentation to study the modification of these films. The use of photoluminescence spectroscopy can be important to understand the optical and electrical properties and reliability of integrated low-k dielectrics.

Photoluminescence intensity depends on the internal surface area. The correlation between the photoluminescence intensity of 4.3 eV peak and the measured surface area calculated for the films measured immediately after full curing can be seen in SI, Figure S9. Further investigations of luminescence sources are planned, including their correlation with dielectric properties, the reliability of low-k dielectrics, and their evolution during various technological treatments, including the use of plasma and ion irradiation.

Supplementary Materials: The following supporting information can be downloaded at the website of this paper posted on Preprints.org, Table S1: Physical properties of organosilicate glass (OSG) films: first type: both ethylene bridges and methyl terminal groups with different precursor ratios (BTMSE/MTMS = 47/53 and 25/75); second type: a mixture of 1,3,5- and 1,3-benzene groups with a ratio of 1,3,5/1,3 = 1:3, 1,3,5/1,3 = 1:7 and 1,4-benzene bridges without porogen (1,4-BB) and with 30 wt% porogen (1,4-BB-p); third type: contains only methyl terminals without bridging groups (MTMS – without porogen, MTMS-p – with porogen). All films are completely cured in the air; Figure S1: Effect of chemical composition during storage of film (BTMSE/MTMS = 47/53, 20 wt% Brij®30) in clean room environment and after soft oxygen ICP plasma. Loss of $\text{Si}-\text{CH}_3$ groups and

hydrophilization was observed for films by using soft oxygen ICP plasma (remove the chemical residue); Figure S2: FTIR spectra of 1,3,5- and 1,3-benzene bridged ratio of 1:3 (bottom) and 1:7 (top) organosilica films with different porogen concentration s (0–41 wt%), soft bake at 200 °C and hard bake at 400 °C in air; Figure S3: Adsorption-desorption isotherms for determining the value of open porosity, generated by ellipsometric porosimetry, of 1,3,5- and 1,3-benzene bridges ratio of 1:3 (a) and 1:7 (b) organosilica films with different porogen concentrations (17–41 wt%), soft bake at 150 °C and hard bake at 400 °C in air; Figure S4: FTIR spectra of pure 1,4-benzene bridged organosilica films: dense (1,4-BB) and with 30 wt% porogen content 1,4-benzene bridged (1,4-BB-p) organosilica films, both the films were completely cured in air; Figure S5: Adsorption-desorption isotherms for determining the value of open porosity (a) and pore size distribution (b), generated by ellipsometric porosimetry, of pure 1,4-benzene bridged organosilica films: dense (1,4-BB) and with 30 wt% porogen content 1,4-benzene bridged (1,4-BB-p) organosilica films, both the films were cured completely in air; Figure S6: FTIR spectra of pure methyl-terminated organosilicate : dense (MTMS) and with 30 wt% porogen content methyl-terminated (MTMS-p), both the films were cured completely in air; Figure S7: Adsorption-desorption isotherms for determining the value of open porosity (a) and pore size distribution (b), generated by ellipsometric porosimetry, of pure methyl-terminated organosilica films: dense (MTMS) and with 30 wt% porogen content methyl terminated (MTMS-p) organosilica films, both the films were cured completely in the air; Figure S8: UV induced PL spectra measured at the different excitation energy for the ethylene bridged films (BTMSE/MTMS = 47/53); Figure S9: Correlation between 4.3 eV UV induced (upon excitation with light of 6.2 eV) room temperature PL emission with the measured surface area in hard baked OSG low-k films containing both methyl terminal and ethylene bridging groups (BTMSE/MTMS ratio of 25/75) with different porosity. However, the PL bands at 2.9, 3.3 and 4.85 eV have the highest intensity in highly porous films. It can be assumed that the reason is that the terminal methyl groups and hydrocarbon residues are mainly located on the pore wall surface. However, this assumption needs further study.

Author Contributions: Conceptualization, M.R.B.; data curation, M.R., J.Z., D.A.S., S.N. and A.S.V.; formal analysis, M.R., J.M.Z., D.A.S., S.N. and A.S.V; funding acquisition, A.S.V, K.A.V., J.Z. and M.R.B.; investigation, M.R.B.; methodology, M.R., J.Z., D.A.S., S.N. and A.S.V; project administration, J.Z. and M.R.B.; resources, J.Z.; supervision, K.A.V., J.Y., J.Z. and M.R.B.; validation, M.R., J.M.Z., D.A.S., S.N. and A.S.V. and M.R.B.; visualization, M.R.; writing: original draft, M.R. and M.R.B.; writing: review & editing, M.R., A.S.V. and M.R.B. All authors have read and agreed to the published version of the manuscript.

Funding: This research was funded by Russian Science Foundation, grant number 23–79–30016; R&D Program of Beijing Municipal Education Commission, grant number KZ202210009014. The APC was funded by R&D Program of Beijing Municipal Education Commission.

Data Availability Statement: Data sharing is not applicable to this article.

Acknowledgments: It is our pleasure to thank Dmitry Seregin, Yingjie Wang, Chunhui Liu, Haoyu Xu and Xuesong Wang for the help in samples preparation and FTIR analysis.

Conflicts of Interest: The authors declare no conflict of interest.

References

1. Van Der Voort, P.; Esquivel, D.; De Canck, E.; Goethals, F.; Van Driessche, I.; Romero-Salguero, F.J. Periodic Mesoporous Organosilicas: from simple to complex bridges; a comprehensive overview of functions, morphologies and applications. *Chem. Soc. Rev.* **2013**, *42*, 3913–3955, doi:10.1039/C2CS35222B.
2. Baklanov, M.R.; Ho, P.S.; Zschech, E. *Advanced Interconnects for ULSI Technology*; Baklanov, M.R., Ho, P.S., Zschech, E., Eds.; John Wiley & Sons, Ltd: Chichester, UK, 2012; ISBN 9781119963677.
3. Kondoh, E. Structural Change in Porous Silica Thin Film after Plasma Treatment. *Electrochem. Solid-State Lett.* **1999**, *1*, 224, doi:10.1149/1.1390693.
4. Devine, R.A.B.; Ball, D.; Rowe, J.D.; Tringe, J.W. Irradiation and Humidity Effects on the Leakage Current in $\text{SiO}_x(\text{CH}_3)_y$ -Based Intermetal Dielectric Films. *J. Electrochem. Soc.* **2003**, *150*, F151, doi:10.1149/1.1586926.
5. Marsik, P.; Verdonck, P.; De Roest, D.; Baklanov, M.R. Porogen residues detection in optical properties of low-k dielectrics cured by ultraviolet radiation. *Thin Solid Films* **2010**, *518*, 4266–4272, doi:10.1016/j.tsf.2009.12.110.
6. Baklanov, M.R.; Zhao, L.; Besien, E. Van; Pantouvaki, M. Effect of porogen residue on electrical characteristics of ultra low-k materials. *Microelectron. Eng.* **2011**, *88*, 990–993, doi:10.1016/j.mee.2010.12.077.
7. Van Besien, E.; Pantouvaki, M.; Zhao, L.; De Roest, D.; Baklanov, M.R.; Tókei, Z.; Beyer, G. Influence of porosity on electrical properties of low-k dielectrics. *Microelectron. Eng.* **2012**, *92*, 59–61, doi:10.1016/j.mee.2011.04.015.

8. Kikkawa, T.; Kuroki, S.; Sakamoto, S.; Kohmura, K.; Tanaka, H.; Hata, N. Influence of Humidity on Electrical Characteristics of Self-Assembled Porous Silica Low- κ Films. *J. Electrochem. Soc.* **2005**, *152*, G560, doi:10.1149/1.1931428.
9. Li, Y.; Ciofi, I.; Carbonell, L.; Heylen, N.; Van Aelst, J.; Baklanov, M.R.; Groeseneken, G.; Maex, K.; Tkei, Z. Influence of absorbed water components on SiOCH low- κ reliability. *J. Appl. Phys.* **2008**, *104*, 034113, doi:10.1063/1.2966578.
10. Biswas, N.; Lubguban, J.A.; Gangopadhyay, S. Electric field and temperature-induced removal of moisture in nanoporous organosilicate films. *Appl. Phys. Lett.* **2004**, *84*, 4254–4256, doi:10.1063/1.1757019.
11. Ogawa, E.T.; Aubel, O. Electrical Breakdown in Advanced Interconnect Dielectrics. In *Advanced Interconnects for ULSI Technology*; John Wiley & Sons, Ltd: Chichester, UK, 2012; pp. 369–434 ISBN 9780470662540.
12. Wu, C.; Li, Y.; Baklanov, M.R.; Croes, K. Electrical Reliability Challenges of Advanced Low- κ Dielectrics. *ECS J. Solid State Sci. Technol.* **2015**, *4*, N3065–N3070, doi:10.1149/2.0091501jss.
13. Jousseaume, V.; Zenasni, A.; Favennec, L.; Gerbaud, G.; Bardet, M.; Simon, J.P.; Humbert, A. Comparison Between E-beam and Ultraviolet Curing to Perform Porous a-SiOC:H. *J. Electrochem. Soc.* **2007**, *154*, G103, doi:10.1149/1.2667980.
14. Gates, S.M.; Neumayer, D.A.; Sherwood, M.H.; Grill, A.; Wang, X.; Sankarapandian, M. Preparation and structure of porous dielectrics by plasma enhanced chemical vapor deposition. *J. Appl. Phys.* **2007**, *101*, 094103, doi:10.1063/1.2718278.
15. Gerbaud, G.; Hediger, S.; Bardet, M.; Favennec, L.; Zenasni, A.; Beynet, J.; Gourhant, O.; Jousseaume, V. Spin-coated and PECVD low dielectric constant porous organosilicate films studied by 1D and 2D solid-state NMR. *Phys. Chem. Chem. Phys.* **2009**, *11*, 9729, doi:10.1039/b909654j.
16. Sinha, H.; Ren, H.; Nichols, M.T.; Lauer, J.L.; Tomoyasu, M.; Russell, N.M.; Jiang, G.; Antonelli, G.A.; Fuller, N.C.; Engelmann, S.U.; et al. The effects of vacuum ultraviolet radiation on low- κ dielectric films. *J. Appl. Phys.* **2012**, *112*, 111101, doi:10.1063/1.4751317.
17. Afanas'ev, V. V.; Nguyen, A.P.D.; Houssa, M.; Stesmans, A.; Tókei, Z.; Baklanov, M.R. High-resolution electron spin resonance analysis of ion bombardment induced defects in advanced low- κ insulators ($\kappa = 2.0\text{--}2.5$). *Appl. Phys. Lett.* **2013**, *102*, 172908, doi:10.1063/1.4801938.
18. King, S.W.; French, B.; Mays, E. Detection of defect states in low- κ dielectrics using reflection electron energy loss spectroscopy. *J. Appl. Phys.* **2013**, *113*, 044109, doi:10.1063/1.4788980.
19. Baklanov, M.R.; Jousseaume, V.; Rakimova, T. V.; Lopaev, D. V.; Mankelevich, Y.A.; Afanas'ev, V. V.; Shohet, J.L.; King, S.W.; Ryan, E.T. Impact of VUV photons on SiO₂ and organosilicate low- κ dielectrics: General behavior, practical applications, and atomic models. *Appl. Phys. Rev.* **2019**, *6*, 011301, doi:10.1063/1.5054304.
20. Mutch, M.J.; Pomorski, T.; Bittel, B.C.; Cochrane, C.J.; Lenahan, P.M.; Liu, X.; Nemanich, R.J.; Brockman, J.; French, M.; Kuhn, M.; et al. Band diagram for low- κ /Cu interconnects: The starting point for understanding back-end-of-line (BEOL) electrical reliability. *Microelectron. Reliab.* **2016**, *63*, 201–213, doi:10.1016/j.microrel.2016.04.004.
21. Pustovarov, V.A.; Zatsepin, A.F.; Biryukov, D.Y.; Aliev, V.S.; Iskhakzay, R.M.K.; Gritsenko, V.A. Synchrotron-Excited Luminescence and Converting of Defects and Quantum Dots in Modified Silica Films. *J. Non. Cryst. Solids* **2023**, *602*, 122077, doi:10.1016/j.jnoncrysol.2022.122077.
22. Skuja, L. Optically active oxygen-deficiency-related centers in amorphous silicon dioxide. *J. Non. Cryst. Solids* **1998**, *239*, 16–48, doi:10.1016/S0022-3093(98)00720-0.
23. Salh, R. Defect Related Luminescence in Silicon Dioxide Network: A Review. In *Crystalline Silicon - Properties and Uses*; InTech, 2011; pp. 135–172.
24. Gismatulin, A.A.; Gritsenko, V.A.; Seregin, D.S.; Vorotilov, K.A.; Baklanov, M.R. Charge transport mechanism in periodic mesoporous organosilica low- κ dielectric. *Appl. Phys. Lett.* **2019**, *115*, 082904, doi:10.1063/1.5113633.
25. Perevalov, T. V.; Gismatulin, A.A.; Seregin, D.S.; Wang, Y.; Xu, H.; Kruchinin, V.N.; Spesivcev, E. V.; Gritsenko, V.A.; Nasirov, K.A.; Prosvirin, I.P.; et al. Critical properties and charge transport in ethylene bridged organosilica low- κ dielectrics. *J. Appl. Phys.* **2020**, *127*, 195105, doi:10.1063/1.5145239.
26. Grill, A.; Gates, S.M.; Ryan, T.E.; Nguyen, S. V.; Priyadarshini, D. Progress in the development and understanding of advanced low κ and ultralow κ dielectrics for very large-scale integrated interconnects—State of the art. *Appl. Phys. Rev.* **2014**, *1*, 011306, doi:10.1063/1.4861876.
27. Dag, Ö.; Yoshina-Ishii, C.; Asefa, T.; MacLachlan, M.J.; Grondey, H.; Coombs, N.; Ozin, G.A. Oriented Periodic Mesoporous Organosilica (PMO) Film with Organic Functionality Inside the Channel Walls. *Adv. Funct. Mater.* **2001**, *11*, 213–217, doi:10.1002/1616-3028(200106)11:3<213::AID-ADFM213>3.0.CO;2-C.
28. Dubois, G.; Volksen, W.; Magbitang, T.; Sherwood, M.H.; Miller, R.D.; Gage, D.M.; Dauskardt, R.H. Superior mechanical properties of dense and porous organic/inorganic hybrid thin films. *J. Sol-Gel Sci. Technol.* **2008**, doi:10.1007/s10971-008-1776-2.

29. Hoffmann, F.; Cornelius, M.; Morell, J.; Fröba, M. Silica-Based Mesoporous Organic-Inorganic Hybrid Materials. *Angew. Chemie Int. Ed.* **2006**, *45*, 3216–3251, doi:10.1002/anie.200503075.

30. Dubois, G.; Volksen, W.; Magbitang, T.; Miller, R.D.; Gage, D.M.; Dauskardt, R.H. Molecular Network Reinforcement of Sol–Gel Glasses. *Adv. Mater.* **2007**, *19*, 3989–3994, doi:10.1002/adma.200701193.

31. Li, H.; Knaup, J.M.; Kaxiras, E.; Vlassak, J.J. Stiffening of organosilicate glasses by organic cross-linking. *Acta Mater.* **2011**, *59*, 44–52, doi:10.1016/j.actamat.2010.08.015.

32. Vanstreels, K.; Wu, C.; Baklanov, M.R. Mechanical Stability of Porous Low-k Dielectrics. *ECS J. Solid State Sci. Technol.* **2015**, *4*, N3058–N3064, doi:10.1149/2.0071501jss.

33. Burg, J.A.; Oliver, M.S.; Frot, T.J.; Sherwood, M.; Lee, V.; Dubois, G.; Dauskardt, R.H. Hyperconnected molecular glass network architectures with exceptional elastic properties. *Nat. Commun.* **2017**, *8*, 1019, doi:10.1038/s41467-017-01305-w.

34. Goethals, F.; Ciofi, I.; Madia, O.; Vanstreels, K.; Baklanov, M.R.; Detavernier, C.; Van Der Voort, P.; Van Driessche, I. Ultra-low-k cyclic carbon-bridged PMO films with a high chemical resistance. *J. Mater. Chem.* **2012**, *22*, 8281, doi:10.1039/c2jm30312d.

35. Lu, Y.; Fan, H.; Doke, N.; Loy, D.A.; Assink, R.A.; LaVan, D.A.; Brinker, C.J. Evaporation-Induced Self-Assembly of Hybrid Bridged Silsesquioxane Film and Particulate Mesophases with Integral Organic Functionality. *J. Am. Chem. Soc.* **2000**, *122*, 5258–5261, doi:10.1021/ja9935862.

36. Redzheb, M.; Prager, L.; Naumov, S.; Krishtab, M.; Armini, S.; Van Der Voort, P.; Baklanov, M.R. Effect of the C-bridge length on the ultraviolet-resistance of oxycarbosilane low-k films. *Appl. Phys. Lett.* **2016**, *108*, 012902, doi:10.1063/1.4939449.

37. Seregin, D.S.; Naumov, S.; Chang, W.-Y.; Wu, Y.-H.; Wang, Y.; Kotova, N.M.; Vishnevskiy, A.S.; Wei, S.; Zhang, J.; Vorotilov, K.A.; et al. Effect of the C-bridge on UV properties of organosilicate films. *Thin Solid Films* **2019**, *685*, 329–334, doi:10.1016/j.tsf.2019.06.050.

38. Vishnevskiy, A.S.; Naumov, S.; Seregin, D.S.; Wu, Y.H.; Chuang, W.T.; Rasadujjaman, M.; Zhang, J.; Leu, J.; Vorotilov, K.A.; Baklanov, M.R. Effects of methyl terminal and carbon bridging groups ratio on critical properties of porous organosilicate-glass films. *Materials (Basel)* **2020**, *13*, 1–21, doi:10.3390/ma13204484.

39. Rasadujjaman, M.; Wang, Y.; Zhang, L.; Naumov, S.; Attallah, A.G.; Liedke, M.O.; Koehler, N.; Redzheb, M.; Vishnevskiy, A.S.; Seregin, D.S.; et al. A detailed ellipsometric porosimetry and positron annihilation spectroscopy study of porous organosilicate-glass films with various ratios of methyl terminal and ethylene bridging groups. *Microporous Mesoporous Mater.* **2020**, *306*, doi:10.1016/j.micromeso.2020.110434.

40. Rasadujjaman, M.; Zhang, J.; Mogilnikov, K.P.; Vishnevskiy, A.S.; Zhang, J.; Baklanov, M.R. Effect of methyl terminal and ethylene bridging groups on porous organosilicate glass films: FTIR, ellipsometric porosimetry, luminescence dataset. *Data Br.* **2021**, *35*, 106895, doi:10.1016/j.dib.2021.106895.

41. Iacopi, F.; Travaly, Y.; Eyckens, B.; Waldorfried, C.; Abell, T.; Guyer, E.P.; Gage, D.M.; Dauskardt, R.H.; Sajavaara, T.; Houthoofd, K.; et al. Short-ranged structural rearrangement and enhancement of mechanical properties of organosilicate glasses induced by ultraviolet radiation. *J. Appl. Phys.* **2006**, *99*, 053511, doi:10.1063/1.2178393.

42. Rezvanov, A.A.; Vishnevskiy, A.S.; Seregin, D.S.; Schneider, D.; Lomov, A.A.; Vorotilov, K.A.; Baklanov, M.R. Benzene bridged hybrid organosilicate films with improved stiffness and small pore size. *Mater. Chem. Phys.* **2022**, *290*, 126571, doi:10.1016/j.matchemphys.2022.126571.

43. Liu, C.; Lv, C.; Kohler, N.; Wang, X.; Lin, H.; He, Z.; Wu, Y.-H.; Leu, J.; Wei, S.; Zhang, J.; et al. Properties of organosilicate low- k films with 1,3- and 1,3,5-benzene bridges between Si atoms. *Jpn. J. Appl. Phys.* **2020**, *59*, SLLG01, doi:10.35848/1347-4065/ab86dc.

44. Rasadujjaman, M.; Wang, X.; Wang, Y.; Zhang, J.; Arkhincheev, V.E.; Baklanov, M.R. Analytical Study of Porous Organosilicate Glass Films Prepared from Mixtures of 1,3,5- and 1,3-Alkoxy silylbenzenes. *Materials (Basel)* **2021**, *14*, 1881, doi:10.3390/ma14081881.

45. Baklanov, M.R.; Mogilnikov, K.P.; Polovinkin, V.G.; Dultsev, F.N. Determination of pore size distribution in thin films by ellipsometric porosimetry. *J. Vac. Sci. Technol. B Microelectron. Nanom. Struct.* **2000**, *18*, 1385, doi:10.1116/1.591390.

46. Haul, R. S. J. Gregg, K. S. W. Sing: Adsorption, Surface Area and Porosity. Academic Press, London 1982. doi:10.1002/bbpc.19820861019.

47. Chernenko, K.; Kivimäki, A.; Pärna, R.; Wang, W.; Sankari, R.; Leandersson, M.; Tarawneh, H.; Pankratov, V.; Kook, M.; Kukk, E.; et al. Performance and characterization of the FinEstBeAMS beamline at the MAX IV Laboratory. *J. Synchrotron Radiat.* **2021**, *28*, 1620–1630, doi:10.1107/S1600577521006032.

48. Sandeep, S.; Vishnevskiy, A.S.; Raetz, S.; Naumov, S.; Seregin, D.S.; Husiev, A.; Vorotilov, K.A.; Gusev, V.E.; Baklanov, M.R. In-Situ Imaging of a Light-Induced Modification Process in Organo-Silica Films via Time-Domain Brillouin Scattering. *Nanomaterials* **2022**, *12*, 1600, doi:10.3390/nano12091600.

49. Zotovich, A.I.; Zyryanov, S.M.; Lopaev, D. V.; Rezvanov, A.A.; Attallah, A.G.; Liedke, M.O.; Butterling, M.; Bogdanova, M.A.; Vishnevskiy, A.S.; Seregin, D.S.; et al. Modification of Porous Ultralow- k Film by Vacuum Ultraviolet Emission. *ACS Appl. Electron. Mater.* **2022**, *4*, 2760–2776, doi:10.1021/acsaelm.2c00281.

50. Perdew, J.P.; Burke, K.; Ernzerhof, M. Generalized Gradient Approximation Made Simple. *Phys. Rev. Lett.* **1996**, *77*, 3865–3868, doi:10.1103/PhysRevLett.77.3865.

51. Perdew, J.P.; Burke, K.; Ernzerhof, M. Generalized Gradient Approximation Made Simple. *Phys. Rev. Lett.* **1997**, *78*, 1396–1396, doi:10.1103/PhysRevLett.78.1396.

52. Adamo, C.; Barone, V. Toward reliable density functional methods without adjustable parameters: The PBE0 model. *J. Chem. Phys.* **1999**, *110*, 6158–6170, doi:10.1063/1.478522.

53. Jaguar, version 9.6, Schrodinger, Inc. 2017.

54. Naumov, S.; Herzog, B.; Abel, B. Spectra and Photorelaxation of Hydroxyphenyl-benzotriazole-Type UV Absorbers: From Monomers to Nanoparticles. *J. Phys. Chem. A* **2020**, *124*, 625–632, doi:10.1021/acs.jpca.9b09883.

55. Weilbeer, C.; Sickert, M.; Naumov, S.; Schneider, C. The Brønsted Acid-Catalyzed, Enantioselective Aza-Diels-Alder Reaction for the Direct Synthesis of Chiral Piperidones. *Chem. - A Eur. J.* **2017**, *23*, 513–518, doi:10.1002/chem.201604356.

56. Bauernschmitt, R.; Ahlrichs, R. Treatment of electronic excitations within the adiabatic approximation of time dependent density functional theory. *Chem. Phys. Lett.* **1996**, *256*, 454–464, doi:10.1016/0009-2614(96)00440-X.

57. Pollard, W.T.; Friesner, R.A. Efficient Fock matrix diagonalization by a Krylov-space method. *J. Chem. Phys.* **1993**, *99*, 6742–6750, doi:10.1063/1.465817.

58. Everett, D.H. *Adsorption Hysteresis*. In: *The Solid-Gas Interface*; Flood E. A.; New York, 1967;

59. Skuja, L.; Leimane, M.; Bite, I.; Millers, D.; Zolotarjovs, A.; Vitola, V.; Smits, K. Ultraviolet luminescence of polycyclic aromatic hydrocarbons in partially consolidated sol-gel silica glasses. *J. Non. Cryst. Solids* **2022**, *577*, 121325, doi:10.1016/j.jnoncrysol.2021.121325.

60. Zhao, J.; Mao, D.S.; Lin, Z.X.; Jiang, B.Y.; Yu, Y.H.; Liu, X.H.; Wang, H.Z.; Yang, G.Q. Intense short-wavelength photoluminescence from thermal SiO₂ films co-implanted with Si and C ions. *Appl. Phys. Lett.* **1998**, *73*, 1838–1840, doi:10.1063/1.122299.

61. Tabassum, N.; Nikas, V.; Ford, B.; Huang, M.; Kaloyerous, A.E.; Gallis, S. Time-resolved analysis of the white photoluminescence from chemically synthesized SiC_xO_y thin films and nanowires. *Appl. Phys. Lett.* **2016**, *109*, 043104, doi:10.1063/1.4959834.

62. Nikas, V.; Tabassum, N.; Ford, B.; Smith, L.; Kaloyerous, A.E.; Gallis, S. Strong visible light emission from silicon-oxycarbide nanowire arrays prepared by electron beam lithography and reactive ion etching. *J. Mater. Res.* **2015**, *30*, 3692–3699, doi:10.1557/jmr.2015.346.

63. Ford, B.; Tabassum, N.; Nikas, V.; Gallis, S. Strong Photoluminescence Enhancement of Silicon Oxycarbide through Defect Engineering. *Materials (Basel)* **2017**, *10*, 446, doi:10.3390/ma10040446.

64. Koós, M.; Pócsik, I. Photoluminescence in Hydrogenated Amorphous Carbon. In *Physics and Applications of Non-Crystalline Semiconductors in Optoelectronics*; Springer Netherlands: Dordrecht, 1997; pp. 361–378.

65. Liu, C.; Qi, Q.; Seregin, D.S.; Vishnevskiy, A.S.; Wang, Y.; Wei, S.; Zhang, J.; Vorotilov, K.A.; Dultsev, F.N.; Baklanov, M.R. Effect of terminal methyl groups concentration on properties of organosilicate glass low dielectric constant films. *Jpn. J. Appl. Phys.* **2018**, *57*, 07MC01, doi:10.7567/JJAP.57.07MC01.

66. Knolle, W.; Feldman, V.I.; Janovský, I.; Naumov, S.; Mehnert, R.; Langguth, H.; Sukhov, F.F.; Orlov, A.Y. EPR study of methyl and ethyl acrylate radical cations and their transformations in low-temperature matrices. *J. Chem. Soc. Perkin Trans. 2* **2002**, 687–699, doi:10.1039/b105384c.

67. Naumov, S.; Knolle, W.; Naumov, S.; Pöpl, A.; Janovský, I. The Dynamical Behavior of the s-Trioxane Radical Cation—A Low-Temperature EPR and Theoretical Study. *Molecules* **2014**, *19*, 17305–17313, doi:10.3390/molecules191117305.

68. V. V. Afanas'ev, K. Keunen, A. P. D. Nguyen, M. Jivanescu, A. Stesmans, Z. Tokei, M. R. Baklanov, and G. P. Beyer, in Symposium O—Materials, Processes, and Reliability for Advanced Interconnects for Micro- and Nanoelectronics (Mater. Res. Soc. Proc., 2011). In Proceedings of the (Mater. Res. Soc. Proc., 2011); 2011; p. 1335.

69. Nikas, V.; Gallis, S.; Huang, M.; Kaloyerous, A.E.; Nguyen, A.P.D.; Stesmans, A.; Afanas'ev, V. V. The origin of white luminescence from silicon oxycarbide thin films. *Appl. Phys. Lett.* **2014**, *104*, 061906, doi:10.1063/1.4865100.

70. Krishtab, M.; Afanas'ev, V.; Stesmans, A.; De Gendt, S. Leakage current induced by surfactant residues in self-assembly based ultralow-k dielectric materials. *Appl. Phys. Lett.* **2017**, *111*, 032908, doi:10.1063/1.4995241.

Disclaimer/Publisher's Note: The statements, opinions and data contained in all publications are solely those of the individual author(s) and contributor(s) and not of MDPI and/or the editor(s). MDPI and/or the editor(s) disclaim responsibility for any injury to people or property resulting from any ideas, methods, instructions or products referred to in the content.